Mechanically Synthesized Zirconium-based MOFs for Adsorptive Removal of Nerve Agent Simulants

Hosein Ghasempour *, Behnam Habibi, Paria Soleimani Abhari

Department of Chemistry, Faculty of Sciences, Tarbiat Modares University, Tehran, Iran

Editor's note: Metal-organic frameworks (MOFs) have shown great potential for the adsorptive removal of various hazardous compounds due to their high specific surface areas and tunable molecular structures. Ghasempour et al. reported an easy, eco-friendly solvent-assisted mechanochemical grinding method for synthesizing Zr-based MOFs, which exhibit a high removal capacity against organophosphorus nerve agents.

doi: 10.22034/jams.2025.210132

How to cite: H. Ghasempour et al. *Journal of Applied Material Science*, **2025**, *1*, 210132.

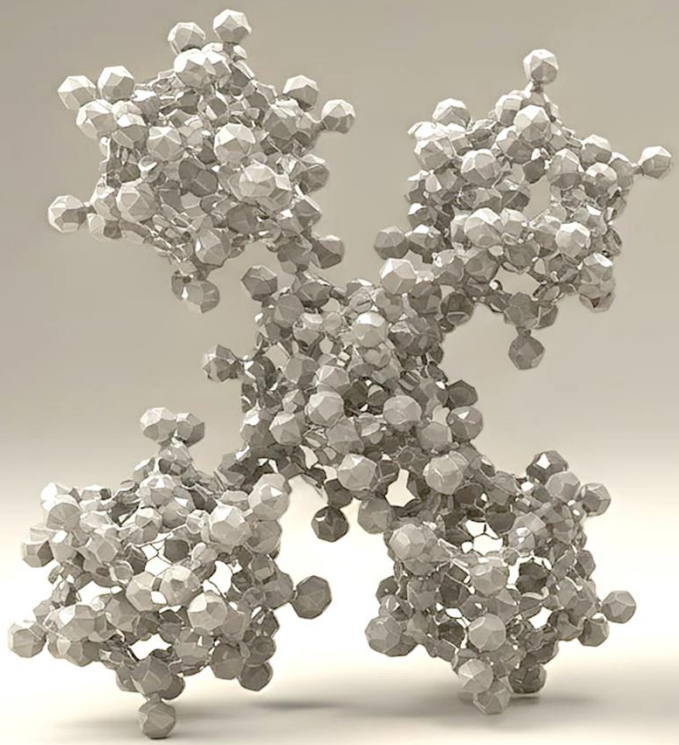

JOURNAL OF
APPLIED
MATERIAL
SCIENCE
jams.hsu.ac.ir

Journal of Applied Material Science **2025**, *1*, 210132
How to cite: H. Ghasempour et al., *Journal of Applied Material Science*, **2025**, *1*, 210132.
Journal homepage: **www.jams.hsu.ac.ir**

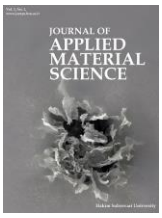

Original Research

Mechanically Synthesized Zirconium-based MOFs for Adsorptive Removal of Nerve Agent Simulants

Hosein Ghasempour *, Behnam Habibi, Paria Soleimani Abhari

Department of Chemistry, Faculty of Sciences, Tarbiat Modares University, Tehran, Iran

Abstract

In this study, two zirconium-based metal-organic frameworks (Zr-MOFs), namely UiO-66 and NH_2-UiO-66, were synthesized using a simple, fast, and eco-friendly solvent-assisted grinding (mechanochemically) approach. The purity and quality of prepared Zr-MOFs were fully characterized via powder X-ray diffraction (PXRD), Fourier transform infrared (FT-IR) spectroscopy, and N_2 adsorption/desorption analyses. Due to its structural similarity to phosphorus nerve agents, dimethyl methylphosphonate (DMMP) was used in this study as the model nerve agent to evaluate the adsorption capacity of prepared Zr-MOFs toward nerve agents. Photoluminescence (PL) spectroscopy was employed to monitor the DMMP concentration during the removal process. Adsorption capacity values of 667 and 834 mg/g were obtained for UiO-66 and NH_2-UiO-66, respectively, indicating their strong interaction with phosphorus nerve agents. Furthermore, the stability and recyclability of the absorbents after the absorption process were confirmed using FT-IR and PXRD results, confirming that Zr-MOFs are perfect candidates for applications related to chemical warfare protection.

Keywords: Metal-organic frameworks; Phosphorus nerve agents; DMMP; Adsorptive removal.

1. Introduction

Chemical warfare agents (CWAs) are a class of chemicals designed to kill, harm, or incapacitate human beings [1]. More than 70 types of compounds have been employed or stored as CWAs in liquid, gas, or solid form during the 20th century [2]. CWA can be categorized based on their biological effects on human health. They may also be classified by their chemical structure or their strategic purpose. Some of the most known CWAs are blister agents, pulmonary/choking agents, blood agents, nerve agents, vomiting agents, and incapacitating agents. It is crucial to take precautions to avoid exposure to these agents.

Among various types of CWAs, organophosphorus nerve agents (OPNs) are considered a serious hazard to living organisms due to their high production rate as a byproduct in phosphorus pesticide manufacturing. One of the distinguishing features of OPNs, compared to other CWAs, is their extreme toxicity, which arises from their ability to bind to the acetylcholinesterase enzyme (AChE) in the synaptic space, leading to neurological impairment and ultimately death [3]. The reactivity of

* Corresponding author.
Email addresses: h.ghasempour@modares.ac.ir, h.ghasempoor92@gmail.com (H. Ghasempour)

Received 9 January 2025
Revised 30 January 2025
Accepted 31 January 2025
Available online 1 February 2025

https://doi.org/10.22034/jams.2025.210132

OPNs is related to their similarity in structure to organophosphate esters, which contain a P=O group, a leaving group (X), and two alkyl/alkoxy substituents (Scheme 1a).

Due to their structural similarity, phosphonate ester pesticides such as paraoxon, and dimethyl nitrophenyl phosphate (DMNP) have been extensively studied as G-type nerve agents, for example, tabun (GA), sarin (GB), and soman (GD) (Scheme 1b). Another G-type nerve agent simulant is dimethyl methylphosphate (DMMP), which, despite its structural resemblance to G-type nerve agents, exhibits significantly lower biological toxicity (Scheme 1c). For this reason, DMMP is one of the most commonly used nerve agent alternatives in research studies aimed at counteracting G-type nerve agents [4].

Metal-organic frameworks (MOFs) are a subset of coordination polymers constructed by connecting metal ions to organic ligands through coordination bonds [5]. Some characteristic properties of these materials include their high structural diversity, extremely high porosity, and tunable functionality [6]. MOFs have been considered for diverse applications, such as gas sorption and separation [7, 8], catalysis [9], and drug delivery [10]. In addition, these materials have attracted great attention due to their high potential for adsorptive removal of CWAs and toxic industrial chemicals (TICs) [3, 11]. Many studies have shown that Zirconium (VI)-based MOFs (Zr-MOFs) exhibit remarkable activity in the catalytic hydrolysis of OPNs [12].

The ability of Zr-MOFs to remove simulants of CWAs, such as DMMP, from aqueous environments is contributed to the presence of Zr–OH–Zr moiety on their clusters, which enables them to mimic the phosphodiesterase enzyme with a Zn–OH–Zn active center [13]. Awual et al. evaluated the adsorption of OPNs and their simulants on Zr-MOFs and concluded that OPNs interact with the framework through hydrogen bonding with Zr–OH sites, highlighting the critical role of this type of interaction at low concentrations [14]. In another similar work, Florénzia et al. investigated the impact of the network topology of Zr-MOFs on their adsorption capacity toward OPNs. This study concluded that the topology-based properties of Zr-MOFs, like specific surface area, pore aperture diameter, metal node connectivity, and accessibility to Lewis acidic Zr(VI) nodes, play a critical role in the adsorption and detoxification of sarin [15]. Herein, two classical Zr-MOFs, UiO-66 and NH_2-UiO-66, were mechanochemically fabricated to investigate their performance to remove the DMMP, as a nerve agent simulant from an aqueous solution. For the first time, photoluminescence spectroscopy was employed to study the adsorption of DMMP by Zr-MOFs.

2. Experimental

2.1. Materials

N,N-dimethylformamide (DMF), chloroform ($CHCl_3$), deuterated chloroform ($CDCl_3$), zirconium tetrachloride ($ZrCl_4$), Methanol, ethyl acetate, acetic acid, terephthalic acid (H_2BDC), 2-aminobenzenedicarboxylic acid (NH_2BDC), dimethyl methylphosphonate (DMMP), potassium bromide (KBr), and N-ethylmorpholine were purchased commercially and used without any purification.

2.2. Mechanical Synthesis of Zr-MOFs.

Zr-MOFs were synthesized by grinding method (Figure 1a). In this process, 3 mmol $ZrCl_4$ (0.7 g) and 3 mmol of the organic ligand (0.5 g of H_2BDC and 0.54 g of NH_2BDC for UiO-66 and NH_2-UiO-66, respectively) were ground together for 2 minutes to homogenize the powder. The resulting homogenous mixture was then wetted with 5 drops of DMF solvent. Subsequently, the

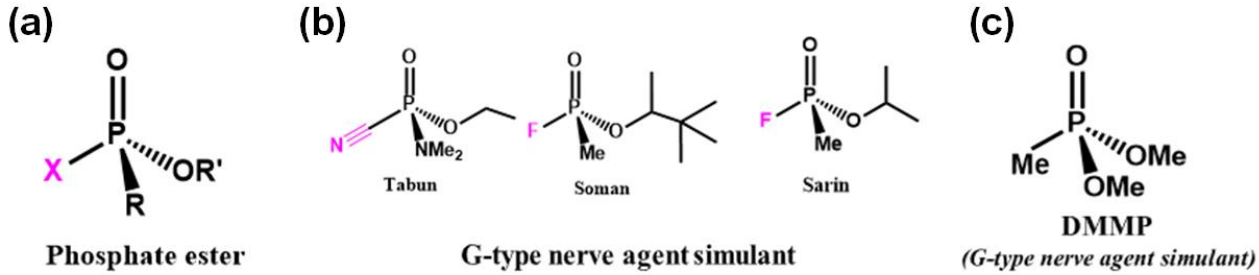

Scheme 1. The chemical structure of (a) phosphate ester, (b) G-type nerve agents, and (c) DMMP as a G-type nerve agent simulant.

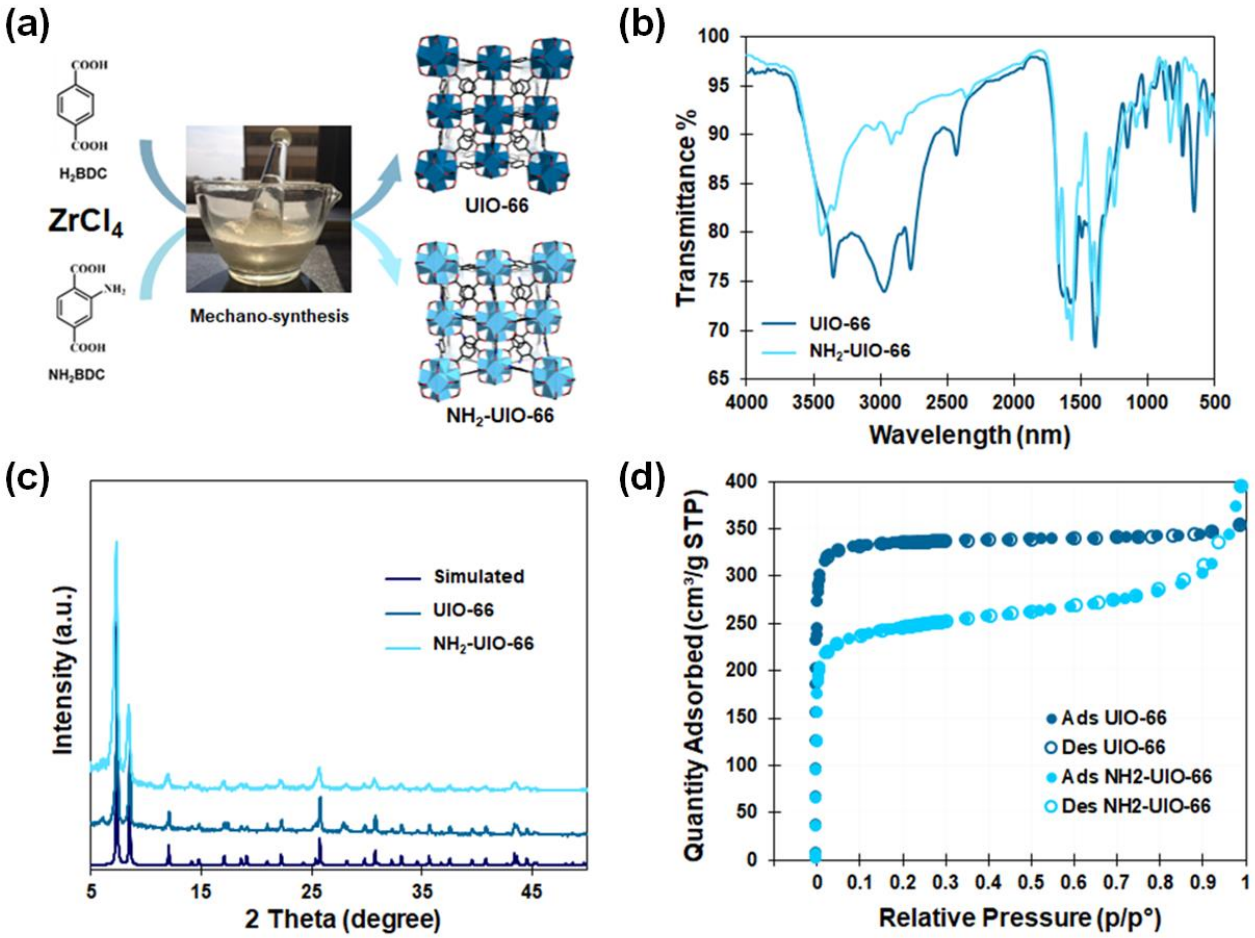

Figure 1. (a) Brief illustration of the mechanical synthesis of Zr-MOFs, characterization of prepared Zr-MOFs with (b) FT-IR, (c) PXRD, and (d) N_2 adsorption/desorption results.

solid-state mechanochemical synthesis was carried out for 30 minutes. The obtained powder was washed three times with a trace volume of DMF to eliminate the unreacted initial precursors. The washed sample was dried in a preheated oven under 100 °C and activated through vacuum degassing at 120 °C overnight.

2.3. Measurements

The materials were weighed using an analytical Sartorius balance with an accuracy of one milligram. Powder X-ray diffraction (PXRD) patterns were obtained using a Philips X'Pert diffractometer with a CuKα X-ray source (λ = 1.54 Å) over a 2θ range of 3–70°. Fourier transform infrared (FT-IR) spectra were recorded on a Thermo Nicolet FTS-7 spectrometer using the KBr pellet technique. UV spectra were collected using a Varian Cary 50 spectrophotometer. The nitrogen (N_2) sorption measurements were performed using a Micromeritics TriStar II 3020 volumetric gas adsorption instrument to calculate the BET surface area. A Perkin Elmer LS-5 luminescence spectrometer was employed to record the fluorescence emission spectra. A Hettich EBA20 centrifuge made in Germany was used for the centrifugation.

To evaluate the removal efficiency of adsorbents toward DMMP, 50 milligrams of Zr-MOFs were added to a DMMP solution in varying concentrations (100-800 ppm) and allowed to equilibrate under ambient conditions. The PL spectrum of the adsorbent-DMMP mixture was then measured to determine the adsorption capacity. The removal efficiency (R %) and adsorption capacity (Q_e, mg/g) of the adsorbent at equilibrium were calculated using equations (1) and (2), respectively:

$$R\ \% = ((C_0 - C_e)/C_0) \times 100 \quad (1)$$

$$Q_e = (C_0 - C_e)\, V/m \quad (2)$$

where m, V, C_0, and C_e represent the mass of the adsorbent (mg), the volume of the DMMP solution (mL), and initial and equilibrium concentrations of DMMP (mg/L), respectively.

3. Results and discussion

As shown in Figure 1b, the FT-IR spectra of the as-prepared Zr-MOFs were compared. The evidence for Zr-MOFs formation is the disappearance of the broad band above 2500 cm^{-1}, which corresponds to hydrogen bonding in free organic ligands. Additionally, the presence of absorption bands at 1350-1700 cm^{-1}, corresponding to the symmetric and asymmetric stretching vibrations of the carboxylate groups, confirms the formation of Zr-MOFs. In the FT-IR spectrum of NH_2-UiO-66, a doublet band is observed in the range of 3350–3450 cm^{-1}, which can be attributed to the primary amine (-NH_2) group of the NH_2BDC linker. Moreover, multiple peaks associated with the –COO functional groups of the linkers appeared in the 1400–1650 cm^{-1} region.

A comparison of the experimentally measured PXRD patterns of the synthesized Zr-MOFs and the extracted pattern from the crystallographic data of UiO-66 confirms the successful synthesis of Zr-MOFs (Figure 1c). Moreover, the BET surface area values of UiO-66 and NH_2-UiO-66, determined *via* N_2 adsorption/desorption isotherms at 77 K, were 1323 and 963 m^2/g, respectively (Figure 1d). This range of surface area falls within the reported range for Zr-MOFs [16].

As previously mentioned, despite its high structural and physical similarity to G-type nerve agents, DMMP exhibits significantly lower biological toxicity. For this reason, it is widely used as one of the most common simulants for studying the detection and removal of G-type nerve agents. However, monitoring the concentration of DMMP presents significant challenges, as this material is not readily detectable by UV-Vis spectroscopy and gas chromatography.

Fortunately, according to the literature, DMMP can be easily detected by photoluminescence (PL) spectroscopy in aqueous solution [17]. Studies have shown that this molecule emits a very strong fluorescence emission band around 320 nm under exciting at 290 nm (λ_{max}) wavelength radiation. Therefore, in this study, the adsorption of this nerve agent simulant by UiO-66 and NH_2-UiO-66 adsorbents was investigated using the PL technique.

Combating chemical weapons such as phosphorus nerve agents in real-world conditions, especially in humid environments, presents significant challenges. Therefore, the main objective of this study is to adsorb DMMP from an aqueous environment. To achieve this, the fluorescence properties of DMMP, a simulant for nerve agents, in water need to be investigated. The preliminary test results showed that the fluorescence behavior of DMMP is not significantly dependent on the solvent. Similar to DMSO, the DMMP aqueous solution exhibits strong emission upon excitation. The only difference is that the excitation wavelength required for this strong emission in water is 280 nm instead of 290 nm (λ_{max}) as shown in Figure 2a.

In other words, DMMP exhibits its strongest fluorescence emission band upon excitation with a 280 nm wavelength instead of 290 nm, making it necessary to use a lower excitation wavelength for further work. To ensure that the DMMP fluorescence emission remains stable over time, 10 microliters of 50 ppm DMMP solution were transferred to 4 ml of distilled water in a fluorescence cell and scanned at different time intervals under 280 nm excitation. As illustrated in Figure 2b, there is no observable decrease in the fluorescence emission intensity of DMMP passing time, even after 24 hours.

For the preliminary test, a very small amount of UiO-66 (the tip of a spoon) was added to the same fluorescence cell, and the fluorescence spectrum was recorded again at the same excitation wavelength the next day. Figure 2b shows that the fluorescence emission of DMMP was completely quenched, which could indicate the adsorptive removal of DMMP from the solution by the adsorbent. To calculate the removal efficiency of adsorbents, 50 milligrams of UiO-66 and NH_2-UiO-66 Zr-MOFs were added to DMMP solution with different concentrations (100-800 ppm) and allowed to equilibrate.

The fluorescence spectrum of the adsorbent-DMMP mixture was then measured to investigate the progress of adsorption, as shown in Figures 2c and d. As expected, DMMP shows a significant decrease in the intensity of its fluorescence emission in the presence of

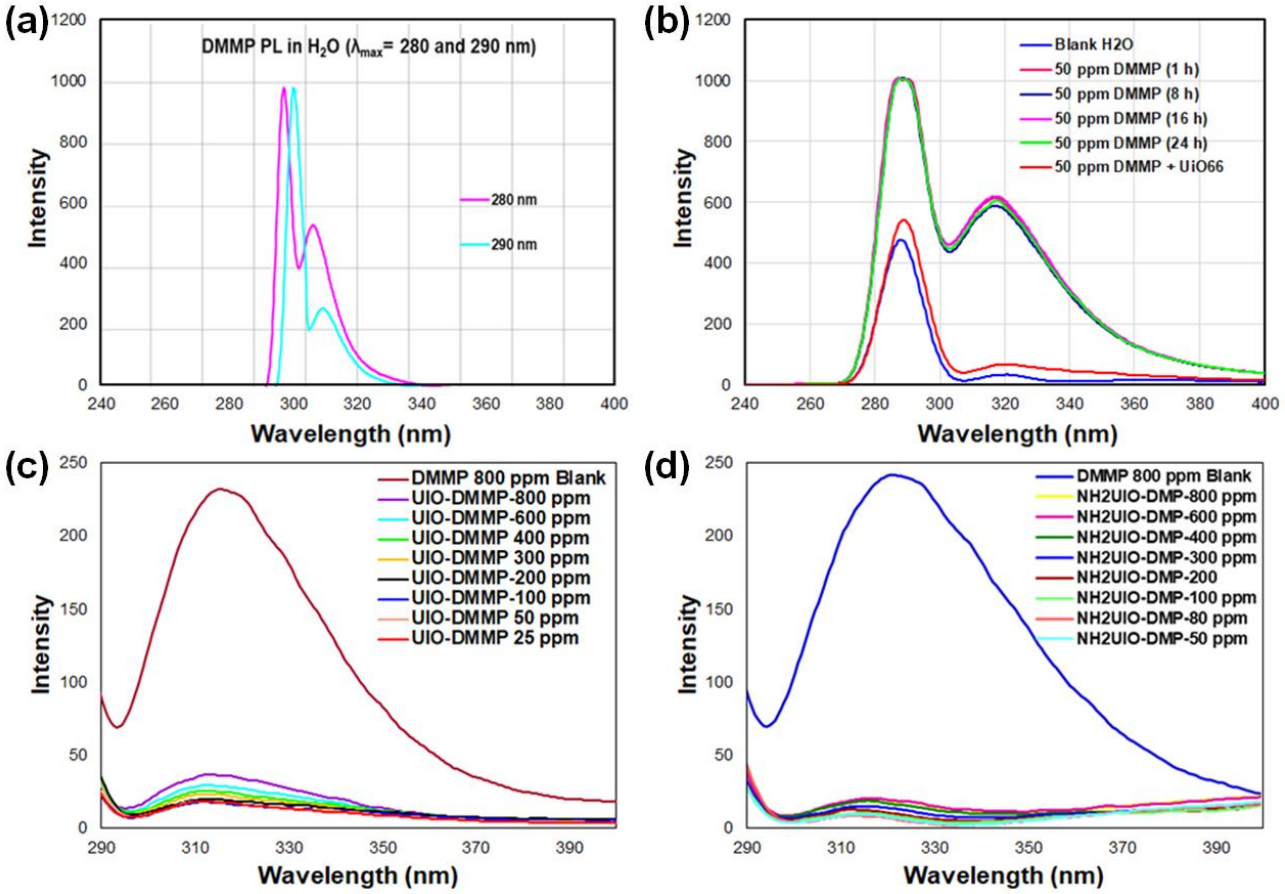

Figure 2. (a) Comparison of fluorescence emission spectra of DMMP in H_2O excited at 280 and 290 nm, (b) fluorescence emission spectra of DMMP in H_2O over time, as well as fluorescence emission spectra of DMMP at different concentrations in the presence of (c) 50 mg UiO-66 and (d) 50 mg NH_2-UiO-66 adsorbent.

the adsorbents, which is also evident from the PL spectra. The data showed that DMMP was completely removed at concentrations up to approximately 200 ppm. However, increasing the concentration above 400 ppm resulted in some remaining DMMP in the environment. The high adsorption capacity of UiO-66 and NH_2-UiO-66 toward DMMP can be identified by comparing the fluorescence emission intensity of blank DMMP solution with that of solution in the presence of the adsorbents at the same 800 ppm concentration (Figures 2c and d).

Based on the results, the intensity of the DMMP fluorescence band is significantly lower in the presence of the adsorbents compared to the control solution. Moreover, the removal efficiency for DMMP removal by UiO-66 and NH_2-UiO-66 is very high. According to equation (1), the removal efficiency for 200, 300, and 400 ppm DMMP concentrations are 97.3%, 89.7%, and 79.1% for the UiO-66 adsorbent, and 98.9%, 95.6%, and 95.3% for the NH_2-UiO-66 adsorbent, respectively. These results indicate that the adsorbents possess a very promising ability to remove DMMP, a pseudo nerve agent, from an aqueous environment, especially NH_2-UiO-66 adsorbent, which demonstrates a higher adsorption capacity than UiO-66 despite its relatively lower surface area.

According to the results, the superior performance of this framework with functionalized pores and surfaces containing free amino groups can be justified. These amino groups facilitate faster and more efficient adsorption of phosphorus nerve agents through increased hydrogen bonding interactions. To study the

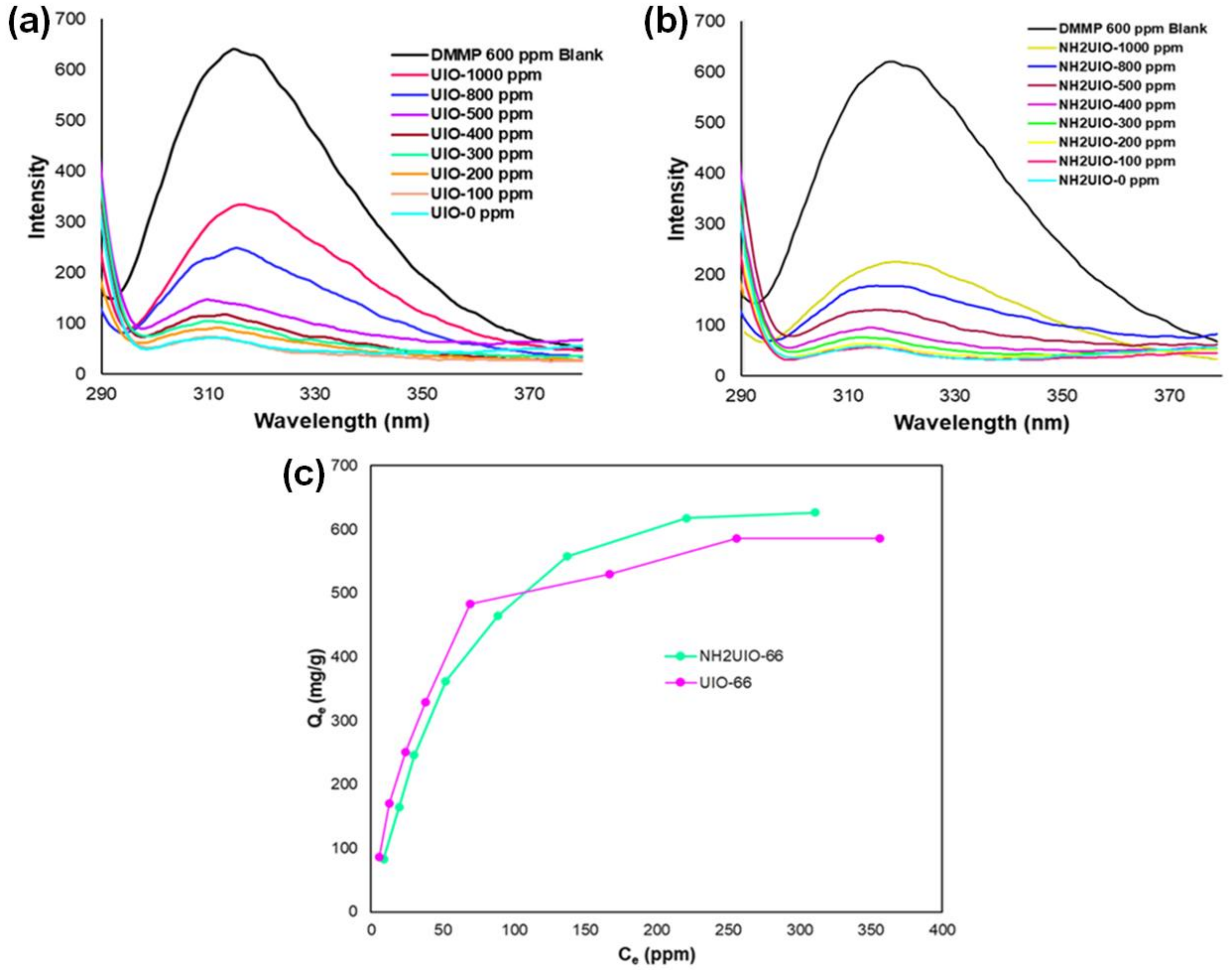

Figure 3. Fluorescence emission spectra of DMMP at different concentrations in the presence of (a) 10 mg UiO-66 and (b) 50 mg NH_2-UiO-66 adsorbent (b); (c) Comparison of the Q_e vs C_e plots for UiO-66 and NH_2-UiO-66 at different DMMP concentration.

adsorption of DMMP accurately and determine the relationship between the adsorption capacity Q_e (mg/g) of the adsorbent and the equilibrium concentration of the adsorbed substance, C_e (mg/L), at a constant temperature, Langmuir and Freundlich isotherm models were used. The equation (3) below shows the linear formula of the Langmuir equation;

$$C_e/q_e = 1/(K_l.q_m) + C_e/q_m \quad (3)$$

where q_m (mg/g) and K_l (L/mg) are the maximum adsorption capacity and the Langmuir adsorption rate constant (which reflects the dependence of adsorbent and adsorbate), respectively. The Freundlich isotherm defines non-ideal and reversible adsorption, which is attributed to multiple-layer adsorption on heterogeneous surfaces. This model can be expressed by equation (4):

$$log\ q_e = log\ K_F + 1/n\ log\ C_e \quad (4)$$

where K_F is the Freundlich constant, and 1/n is the adsorption intensity.

Typically, Langmuir and Freundlich adsorption isotherms provide valuable insights into the adsorption mechanism and behavior of the adsorbent. The Langmuir model defines the reversible chemical equilibrium between the adsorbent surface and the solution. This model adjudges that adsorption occurs uniformly as a monolayer on the surface of the adsorbent and that the adsorbed substance does not penetrate the surface of the adsorbent. The Langmuir isotherm is linear, as represented by equation (2). According to the Langmuir isotherm model, K_l is the Langmuir adsorption rate constant in L/mg, and Q_m is the

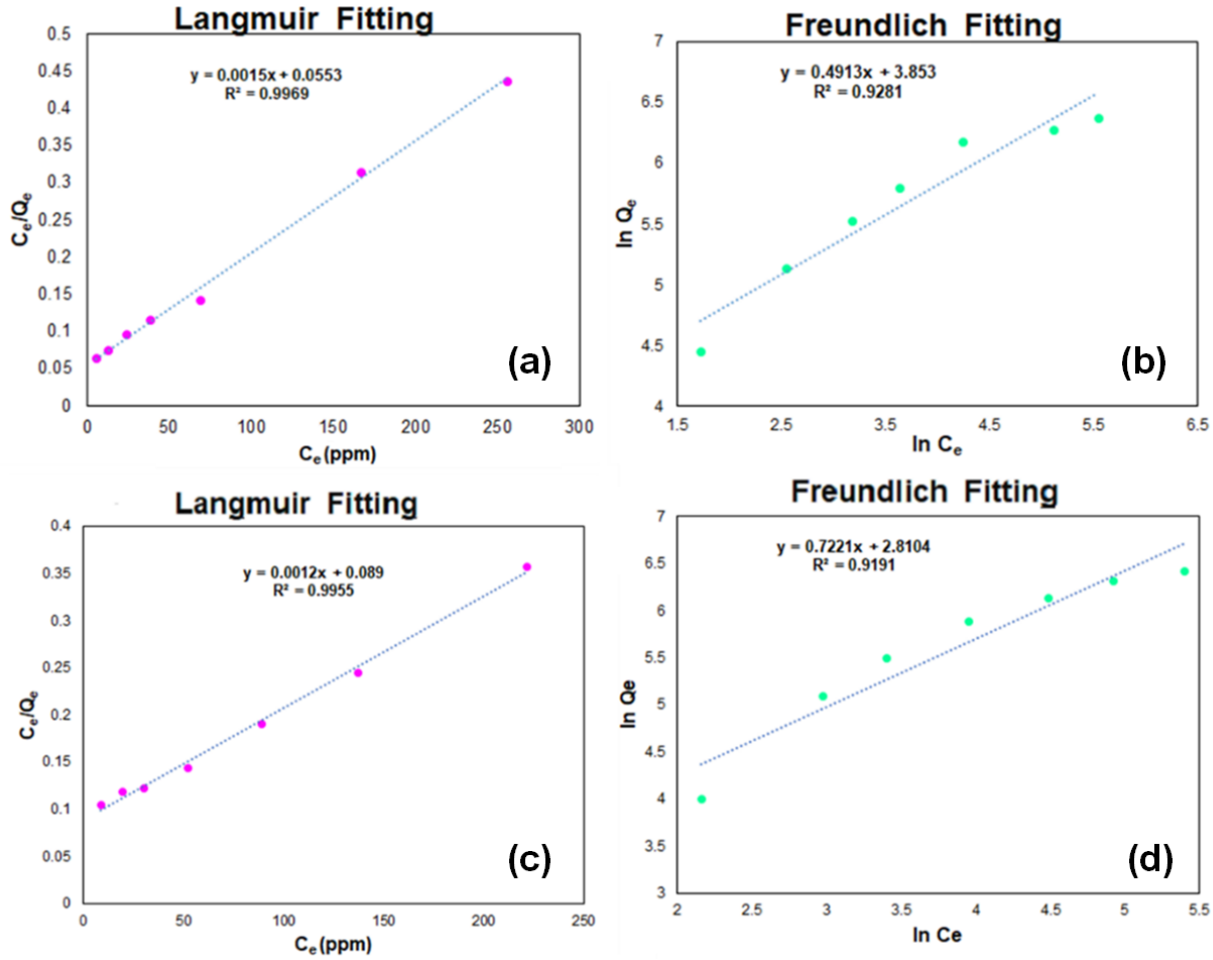

Figure 4. Langmuir and Freundlich fitting of experimental adsorption of DMMP by (a and b) UiO-66 and (c and d) NH_2-UiO-66 adsorbents.

maximum adsorption capacity in mg/g. The Freundlich isotherm is a non-ideal and reversible adsorption model in which adsorption occurs as a non-uniform multilayer on the adsorbent surface. Equation (4) reveals the relationship between adsorption capacity and the adsorbed concentration in the Freundlich adsorption model, where K_F and 1/n are the Freundlich constant and the adsorption intensity, respectively. The value of n also describes the desirability/undesirability of the adsorption intensity respectively.

To calculate the maximum adsorption capacity, 10 mg of the Zr-MOFs were immersed in a DMMP solution with varying concentrations (100-1000 ppm). The fluorescence spectrum of the adsorbent-DMMP mixture was measured to monitor the progress of adsorption, as shown in Figures 3a and b. Interestingly, the intensity of DMMP fluorescence in the 1000 ppm solution was significantly lower in the presence of the adsorbent compared to the control solution with a concentration of 600 ppm.

According to the experimental data, only 10 milligrams of the adsorbent is sufficient to almost completely quench the fluorescence band of DMMP solutions at a concentration of 200 ppm. At first glance, it appears that the adsorption capacity of NH_2-UiO-66 is higher than that of UiO-66. However, to confirm this, the adsorption isotherm, Langmuir and Freundlich plots were drawn. For this purpose, the experimental results obtained from both Langmuir and Freundlich models were evaluated to determine which model corresponds to the adsorption process. The Langmuir plot is obtained by plotting the ratio of equilibrium concentration to the corresponding adsorption capacity (C_e/Q_e) against the equilibrium concentration (C_e), while the Freundlich

diagram is obtained by plotting the natural logarithm of the adsorption capacity (ln Q_e) versus the natural logarithm of the equilibrium concentration (ln C_e) (Figure 4). The obtained correlation coefficients R^2 (0.9969 and 0.9281 for Langmuir and Freundlich models, respectively, for UiO-66 adsorbent, and 0.9955 and 0.9191 for Langmuir and Freundlich models, respectively, for NH_2-UiO-66 adsorbent) indicate that DMMP adsorption by both adsorbents follows the Langmuir model, meaning that DMMP molecules interact uniformly and monolayer on the adsorbent surface and are adsorbed.

Given that the Langmuir adsorption is applicable, equation (3) was used to calculate the maximum adsorption capacity (Q_{max}), where the inverse of the slope is equal to Q_{max}. The calculated adsorption capacities for UiO-66 and NH_2UiO-66 were 667 and 834 mg/g, respectively, indicating the very high potential of these adsorbents for removing phosphorus nerve agents from an aqueous environment. The obtained maximum adsorption capacity for NH_2UiO-66 is approximately 25% higher than that of UiO-66, suggesting that the functional groups in NH_2-UiO-66 significantly enhance the adsorption performance. The only difference between two Zr-MOFs studied is the free amino decorated wall of NH_2-UiO-66 framework (Figure 1a), which can play a critical role in the enhancement of the adsorption capacity.

Using the Langmuir equation, the Langmuir adsorption isotherm can be obtained by plotting the adsorption capacity at equilibrium (Q_e) versus the concentration of DMMP at equilibrium (C_e). Figure 3c shows a comparison of the Langmuir adsorption isotherms for the two adsorbents. As observed, the adsorption behavior of both frameworks is very similar, with the notable difference that at low equilibrium concentrations (0 to 100 ppm), DMMP adsorption by UiO-66 occurs slightly faster than that of NH_2-UiO-66. However, as the concentration increases beyond 500 ppm, the adsorption capacity of NH_2-UiO-66 reaches

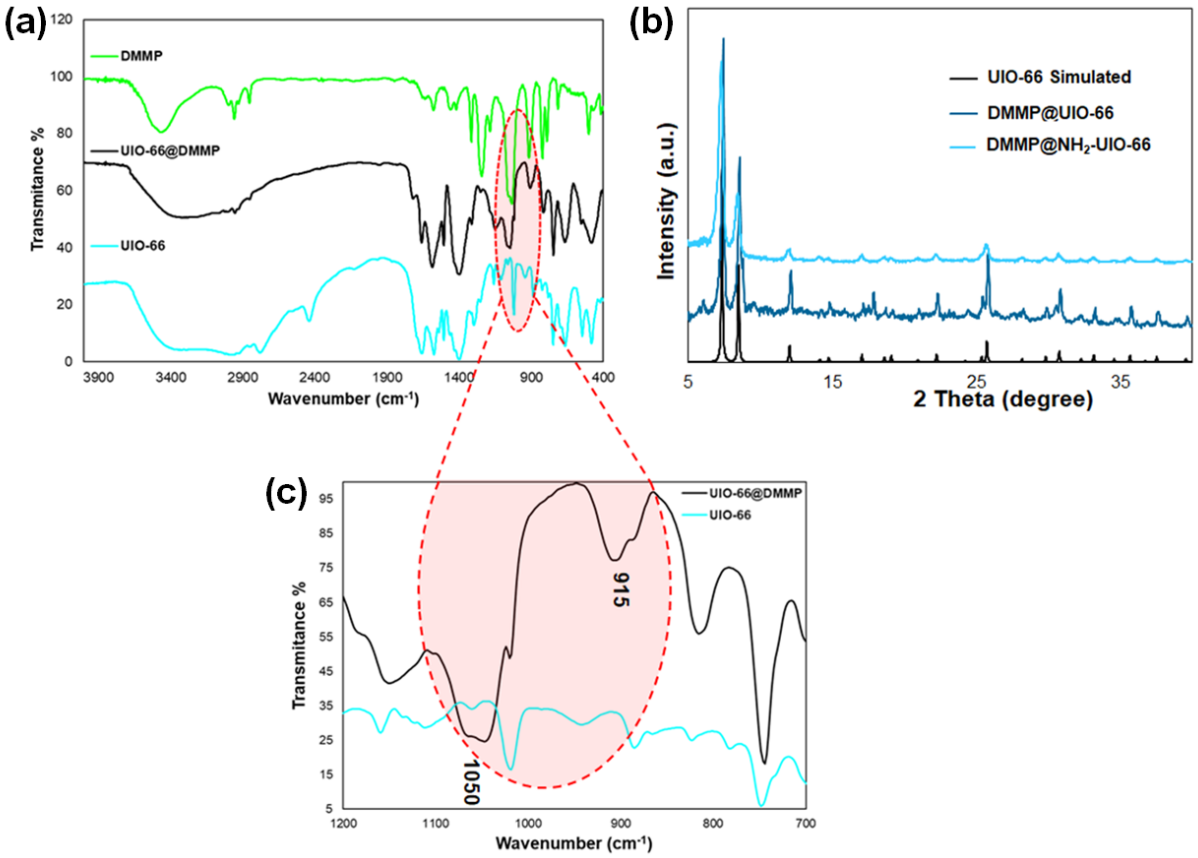

Figure 5. (a) FT-IR spectra of DMMP and UiO-66, before and after the adsorption of DMMP, (b) comparison of the simulated XRD pattern of UiO-66 with experimental PXRD of Zr-MOFs after adsorption of DMMP, and (c) selected wavenumber region of FTIR in panel a for UiO-66, before and after the adsorption of DMMP.

saturation later than UiO-66. This difference in behavior can be attributed to the presence of functional amino groups in the NH_2-UiO-66 framework, which, despite the higher surface area of UiO-66, may contribute to stronger interactions and a slower but more efficient adsorption process at higher concentrations.

FT-IR and PXRD were applied to determine the absorbed DMMP on Zr-MOFs and to investigate the stability of the absorbent after absorption. Figure 5a shows the comparison of FT-IR spectra of DMMP, UiO-66, and DMMP@UiO-66 (after absorption) in the 400 to 2000 nm region. A magnified representation of the FT-IR spectrum in Figure 5c clearly shows two absorption bands at the wavenumbers of 915 and 1050 cm^{-1} in the spectrum of DMMP@UiO-66 (black line), which can be attributed to the P=O and C-P-C bonds in DMMP. These bands are not observed in the spectrum of pristine UiO-66 (blue line), confirming the presence of absorbed DMMP on the surface of the Zr-MOFs. To investigate the stability of the absorbent after absorption, we used the PXRD technique, and the results are presented in Figure 5b. As is evident from the figure, the lack of any shift in the peak positions or any significant decrease in their intensities indicates the stability of UiO-66 and NH_2-UiO-66 absorbents after absorption.

4. Conclusions

This study represented the green fabrication of two famous Zr-based MOFs, UiO-66 and NH_2-UiO-66, using a rapid and simple mechanochemical method, and their performance in adsorptive removal of OPNs. To investigate the ability of these absorbents to remove OPNs, DMMP, was used as a simulant model. Langmuir and Freundlich adsorption models were applied to calculate the maximum adsorption capacity, and it was found that DMMP adsorption by UiO-66 and NH_2-UiO-66 absorbents follows the Langmuir model. The adsorption capacity values for UiO-66 and NH_2-UiO-66 were calculated to be 667 and 834 mg/g, respectively, indicating their high capacity for adsorptive removal of nerve agents from the aqueous environment. Furthermore, the stability and recyclability of the absorbents after the absorption process were confirmed using FT-IR and PXRD techniques, demonstrating that Zr-MOFs are very promising materials to chemical weapon protection.

Conflict of Interest

The author declares no conflict of interest.

References

1. Y.C. Yang, J.A. Baker, and J.R. Ward. Decontamination of chemical warfare agents. *Chemical Reviews*, **1992**, *92*, 1729.
2. J.B. DeCoste and G.W. Peterson. Metal–organic frameworks for air purification of toxic chemicals. *Chemical reviews*, **2014**, *114*, 5695.
3. N.S. Bobbitt, et al. Metal–organic frameworks for the removal of toxic industrial chemicals and chemical warfare agents. *Chemical Society Reviews*, **2017**, *46*, 3357.
4. S. Mukherjee and R.D. Gupta. Organophosphorus nerve agents: types, toxicity, and treatments. *Journal of toxicology*, **2020**, *2020*, 3007984.
5. Q. Bao and K.P. Loh. Graphene photonics, plasmonics, and broadband optoelectronic devices. *ACS nano*, **2012**, *6*, 3677.
6. H. Ghasempour, et al. Metal–organic frameworks based on multicarboxylate linkers. *Coordination Chemistry Reviews*, **2021**, *426*, 213542.
7. J.-R. Li, J. Sculley, and H.-C. Zhou. Metal–organic frameworks for separations. *Chemical reviews*, **2012**, *112*, 869.
8. H. Li, et al. Porous metal-organic frameworks for gas storage and separation: Status and challenges. *EnergyChem*, **2019**, *1*, 100006.
9. J. Jiang and O.M. Yaghi. Brønsted acidity in metal–organic frameworks. *Chemical reviews*, **2015**, *115*, 6966.
10. P. Horcajada, et al. Porous metal–organic-framework nanoscale carriers as a potential platform for drug delivery and imaging. *Nature materials*, **2010**, *9*, 172.
11. L. Rani, et al. A critical review on recent developments in MOF adsorbents for the elimination of toxic heavy metals from aqueous solutions. *Environmental Science and Pollution Research*, **2020**, *27*, 44771.
12. H. Ghasempour and A. Morsali. Function–Topology Relationship in the Catalytic Hydrolysis of a Chemical Warfare Simulant in Two Zr-MOFs. *Chemistry–A European Journal*, **2020**, *26*, 17437.
13. M.J. Katz, et al. Simple and Compelling Biomimetic Metal–Organic Framework Catalyst for the Degradation of Nerve Agent Simulants. *Angew. Chem. Int. Ed.*, **2014**, *53*, 497.

14. A. Michalkova and J. Leszczynski. Interactions of nerve agents with model surfaces: Computational approach. *Journal of Vacuum Science Technology A*, **2010**, *28*, 1010.

15. F.A. Son, et al. Uncovering the Role of Metal–Organic Framework Topology on the Capture and Reactivity of Chemical Warfare Agents. *Chemistry of Materials*, **2020**, *32*, 4609.

16. Y.-H. Huang, et al. Green and rapid synthesis of zirconium metal–organic frameworks via mechanochemistry: UiO-66 analog nanocrystals obtained in one hundred seconds. *Chemical Communications*, **2017**, *53*, 5818.

17. R. Puglisi, et al. Supramolecular recognition of a CWA simulant by metal–salen complexes: the first multi-topic approach. *Chemical Communications*, **2018**, *54*, 11156.

Graphical Abstract